ADVANCED ENERGY MATERIALS

Supporting Information

Increasing the Pressure-Free Stripping Capacity of the Lithium Metal Anode in Solid-State-Batteries by Carbon Nanotubes

Till Fuchs, Catherine G. Haslam, Alexandra C. Moy, Christian Lerch, Thorben Krauskopf, Jeff Sakamoto,* Felix H. Richter,* and Jürgen Janek*

Increasing the Pressure-Free Stripping Capacity of the Lithium Metal Anode in Solid-State-Batteries by Carbon Nanotubes

Till Fuchs[1,2], Catherine G. Haslam[3,4], Alexandra C. Moy[3], Christian Lerch[1,2], Thorben Krauskopf[1,2], Jeff Sakamoto[3,4*], Felix H. Richter[1,2*] and Jürgen Janek[1,2*]

[1]Institute of Physical Chemistry, Justus-Liebig-University Giessen, Heinrich-Buff-Ring 17, D-35392 Giessen, Germany.

[2]Center for Materials Research (ZfM), Justus-Liebig-University Giessen, Heinrich-Buff-Ring 16, D-35392 Giessen, Germany.

[3]Department of Materials Science and Engineering, University of Michigan, Ann Arbor, MI 48109, USA

[4]Department of Mechanical Engineering, University of Michigan, Ann Arbor, MI 48109, USA
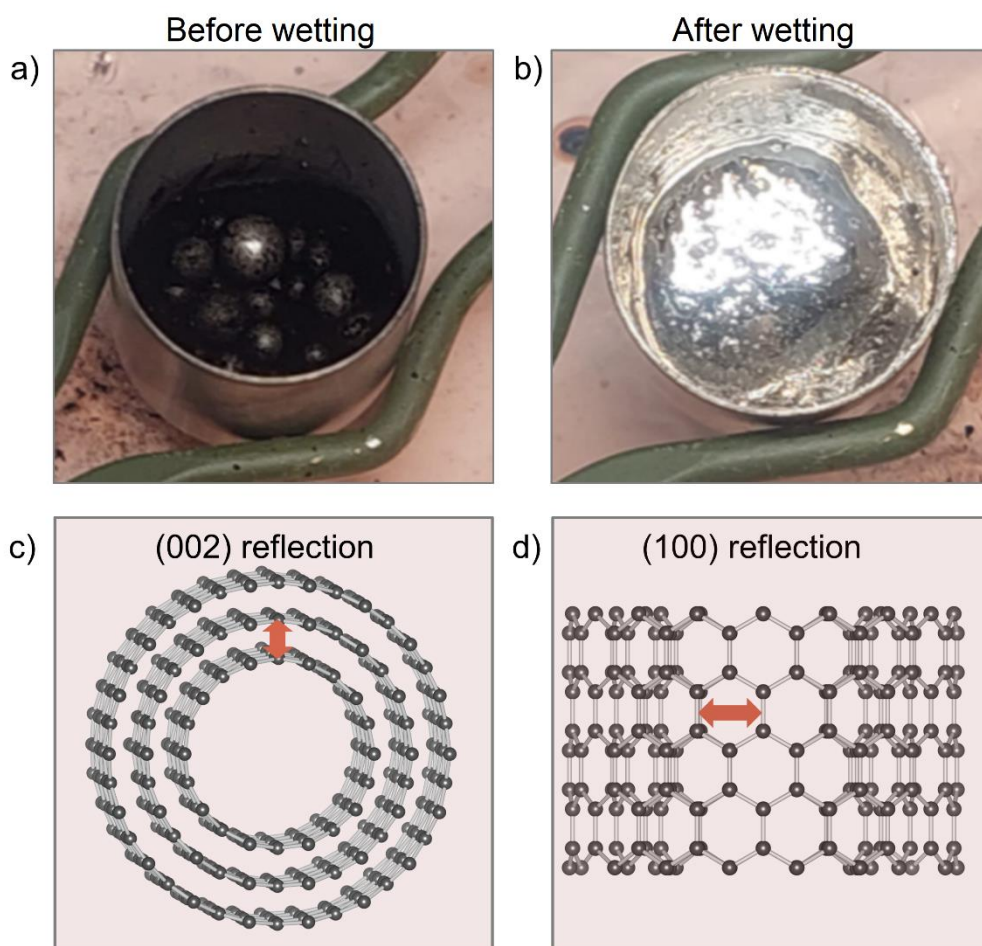
Figure S1. a) Digital photograph of the mixture during dispersing the CNT within liquid lithium at 350 °C. At a certain point during preparation, the CNTs are wetted by liquid lithium, which is shown in b). Differences in wetting are to be expected when other kinds of CNTs are used in dependence of their structure and geometric parameters. c) and d) Schematic explanation of the (002) and (100) reflections of CNT visible in the XRD in Figure 1.

Table S1. Overview of impedance fitting parameters of Li$_{id}$/LLZO/Li-CNT40. The fitted experimental spectrum is shown in Figure 2. The constant phase element Q exhibits the impedance $Z_Q = (i\omega C)^{-\alpha}$ with ω, C and α being the excitation frequency, capacitance and ideality factor thereof, respectively.

Parameter	Value	Error / ±	Typical[1,5]
R_{Bulk} / Ω cm^2	280.0	0.6	-
Q_{Bulk} / F cm^2	$1.65 \cdot 10^{-11}$	$0.01 \cdot 10^{-11}$	$10^{-11} - 10^{-10}$
α_{Bulk}	0.97	0.00	0.9 - 1.0
R_{GB} / Ω cm^2	36.4	4.3	-
Q_{GB} / F cm^2	$3.7 \cdot 10^{-9}$	$1.3 \cdot 10^{-9}$	$10^{-9} - 10^{-8}$
α_{GB}	0.98	0.03	0.8 - 1.0
R_{Int} / Ω cm^2	26.9	4.2	-
Q_{Int} / F cm^2	$3.9 \cdot 10^{-8}$	$8 \cdot 10^{-9}$	$10^{-8} - 10^{-6}$
α_{Int}	0.82	0.04	0.7 - 1.0
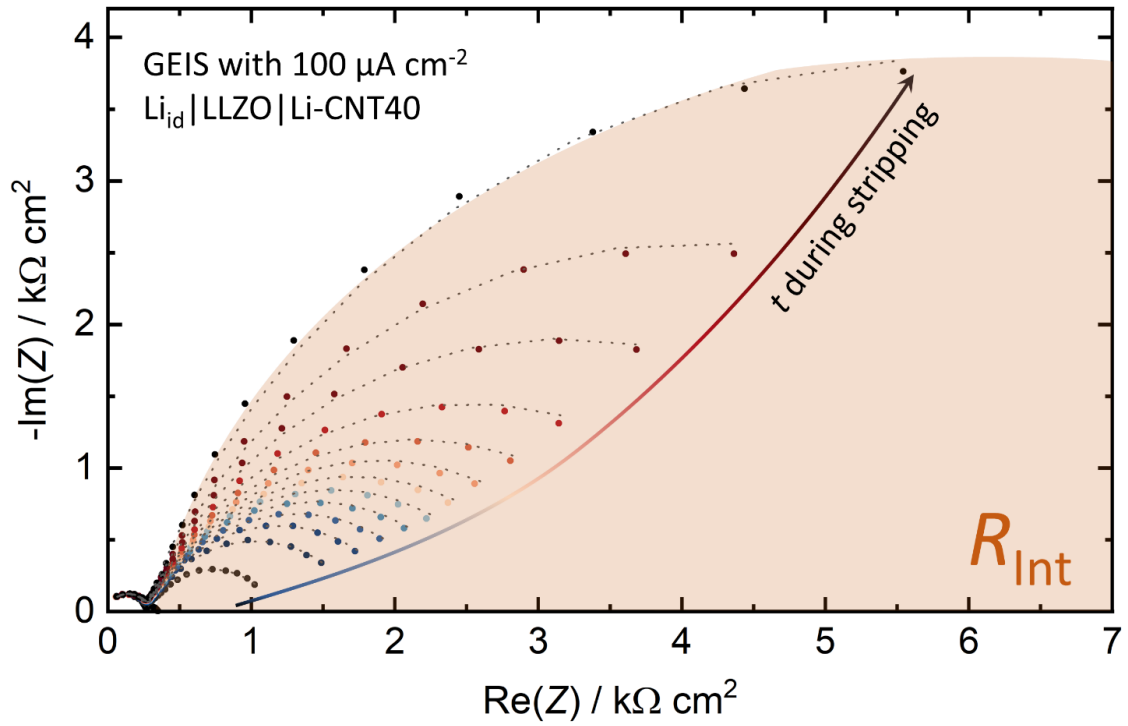
Figure S2. Evolution of the impedance during stripping of Li$_{id}$|LLZO|Li-CNT40 with 100 µA cm^{-2} displayed in selected Nyquist-Plots. Bulk and grain boundary resistance remain constant, indicating that no dendrite growth is taking place.
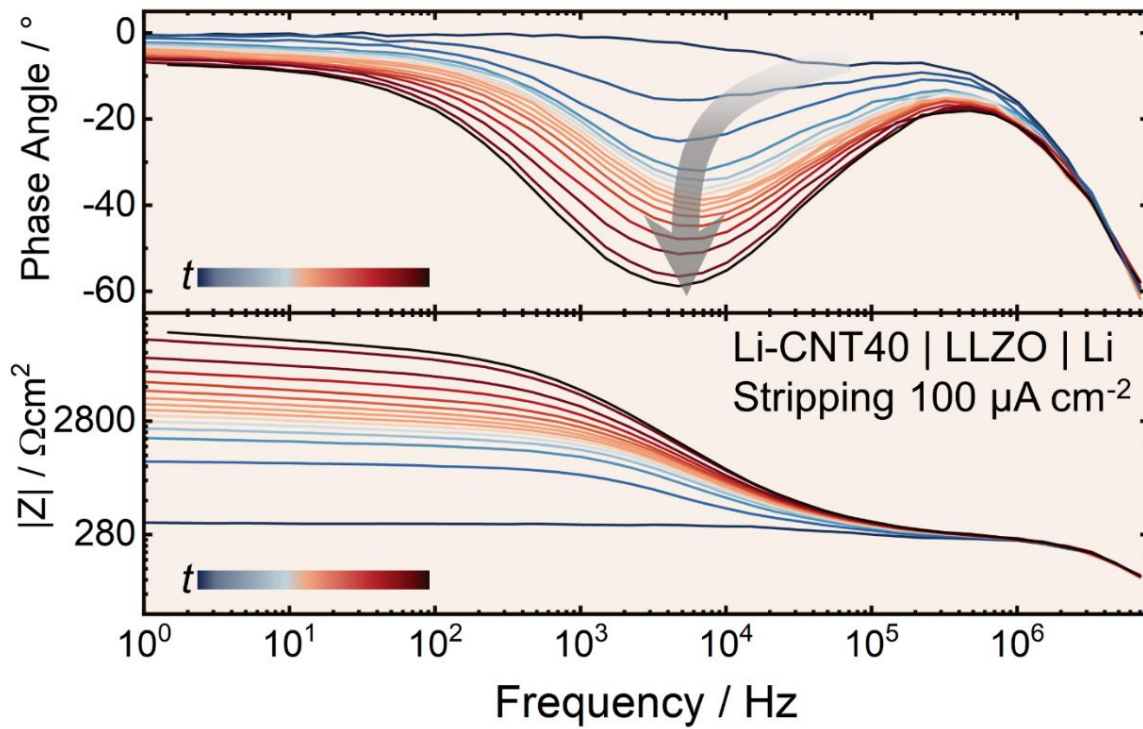
Figure S3. The top figure depicts the phase angle and the bottom one the value of the impedance |Z| versus frequency in a Bode plot. While the time constant of the constriction resistance shifts to higher frequencies for pure lithium electrodes, it remains roughly constant for composite electrodes.[1,2] *This is explained by a more homogenous contact spot distribution for Li-CNT, as also seen with Li-Mg alloys, too. In these cases, the current is more homogeneously distributed, leading to less Joule heating at the contact spots. The bottom graph shows that the overall resistance increase mainly occurs in the low frequency regions below $10^3 – 10^4$ Hz, consistent with the evolution of the Nyquist plots shown in Figure S2.*
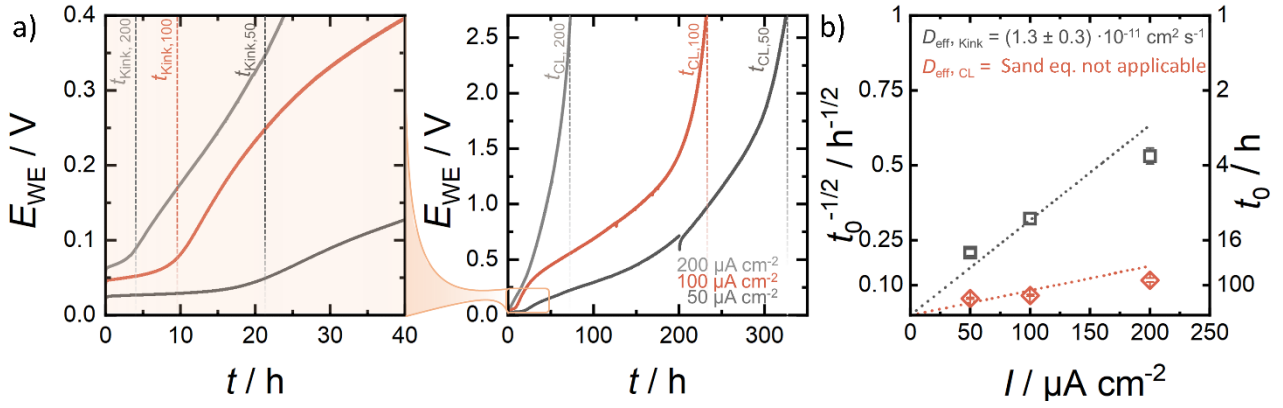
Figure S4. a) Voltage profiles during stripping of Li-CNT30 at different magnifications. The stripping current densities i were chosen as 50 µA cm⁻², 100 µA cm⁻² and 200 µA cm⁻². Dashed lines indicate the times until a distinct change of slope occurs ($t_{Kink, i}$) and until full contact loss is observed ($t_{CL, i}$). To obtain the respective diffusion coefficients via the Sand equation, b) displays a plot of $t_{Kink}^{-1/2}$ and $t_{CL}^{-1/2}$ versus the applied current density. Note that the little discontinuity in a) at 200 h for 50 µA cm⁻² originates from a short pause in data acquisition.

Via the Sand equation

$$\frac{1}{\sqrt{t_i}} = \frac{2}{c_0 F \cdot \sqrt{\pi \cdot D_{\text{eff,j}}}} \cdot i \tag{1}$$

it is possible to calculate an effective diffusion coefficient D_{eff} by plotting $t_i^{-1/2}$ versus the applied current density i.[3,4] Herein, c_0 and t_j denote the initial concentration of lithium inside the material and the time until contact loss occurs during dissolution. However, the values obtained for the contact loss of the composite electrode are flawed, as the electrode thickness d is only slightly larger than the hypothetical thickness of stripped lithium, which leads to the requirement

$$d \gg \sqrt{i_i \cdot D_{\text{eff}}^{-1}} \tag{2}$$

not being fulfilled. This leads to an underestimation of $t_{\text{CL,50}}$ for low current densities, as seen in the orange data point in Figure S4b. Additionally, it is shown that – while the Sand equation describes 1-dimensional diffusion – competing 3D diffusion processes like surface adatom diffusion or diffusion through and along CNTs in this case, play an important role as well. Nevertheless, general and qualitative conclusions about D_{eff} can still be drawn from the time until the kink occurs.

Figure S4a displays the voltage profile during stripping of Li-CNT30 with varying applied current densities. It is reasonable, that with higher current densities, the electrode is depleted faster and a lower capacity is obtained, as also reported for Li-Mg alloys.[2] However, the inflection point within

6

the profile ("kink") also occurs earlier with higher applied current densities. Interestingly, the kink occurs roughly at the same time, when non-composite Li$_{id}$|LLZO interfaces show full contact loss.[2] Using t_{Kink} to calculate an effective diffusion coefficient via Sand's equation, $D_{eff} = (1.3 \pm 0.3) \cdot 10^{-11}$ cm^2 s^{-1} results. The estimated value for D_{eff} should not be mistaken as self-diffusion coefficient of lithium, which does not include the diffusion and creep along defects, such as dislocations, grain boundaries and surfaces. For a detailed overview of diffusion coefficients for lithium obtained by different methods, the reader is referred to a work by Krauskopf et al.[2]

The effective diffusion coefficient calculated from the time until contact is lost cannot be calculated in the manner of the Sand's equation, as the interface is no longer planar beyond the inflection point. Additionally, the condition given in Eq. (2) for Sand's equation to be valid is not fulfilled anymore due to the high amount of lithium being stripped from the electrode.
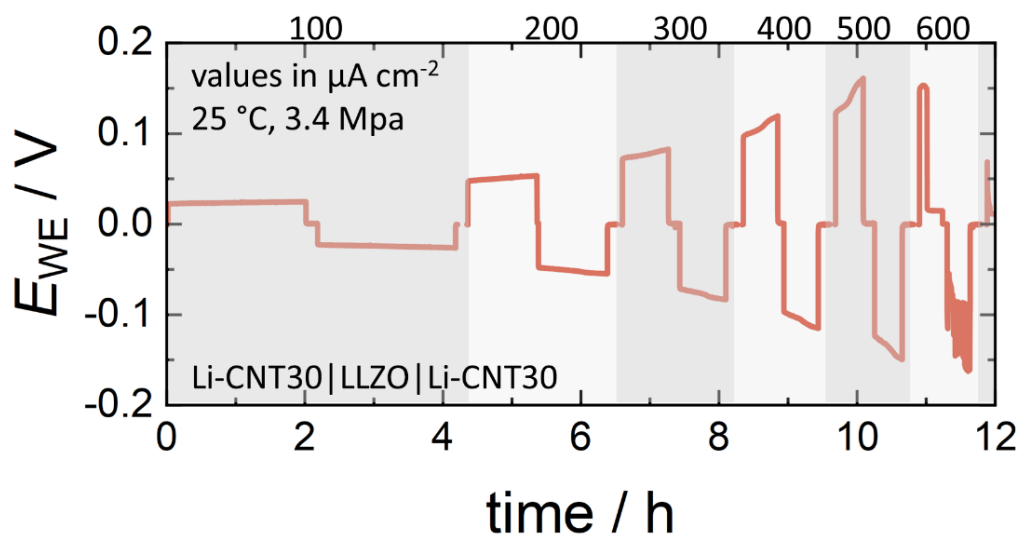
Figure S5. A voltage profile of Li-CNT30|LLZO|Li-CNT30 with increasing current density to obtain a critical current density of about 600 µA cm^{-2} when (dis)charging 0.2 mAh cm^{-2} is shown.
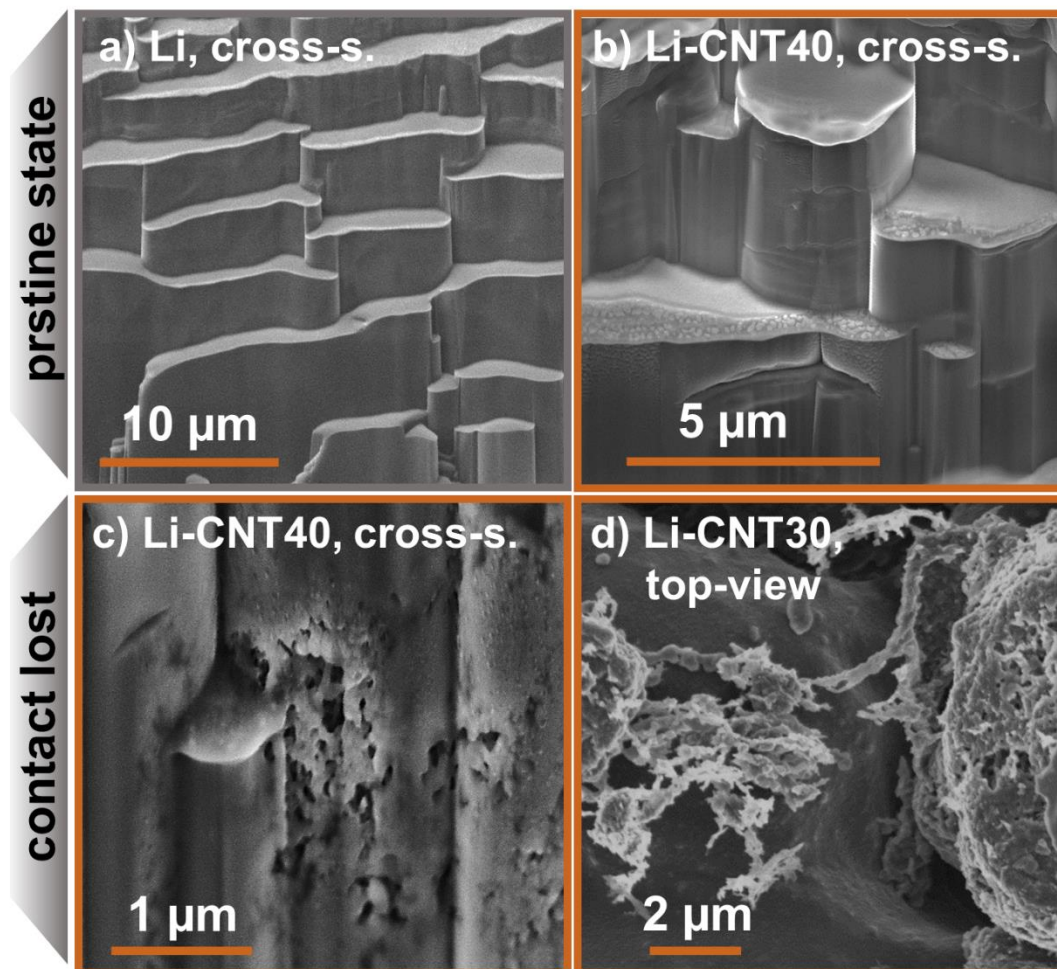
Figure S6. SEM images of a) pristine lithium and b) pristine Li-CNT40 in cross-sectional view. Cross-sectional and top-view SEM images of Li-CNT40 in higher magnifications after stripping are shown in c) and d).
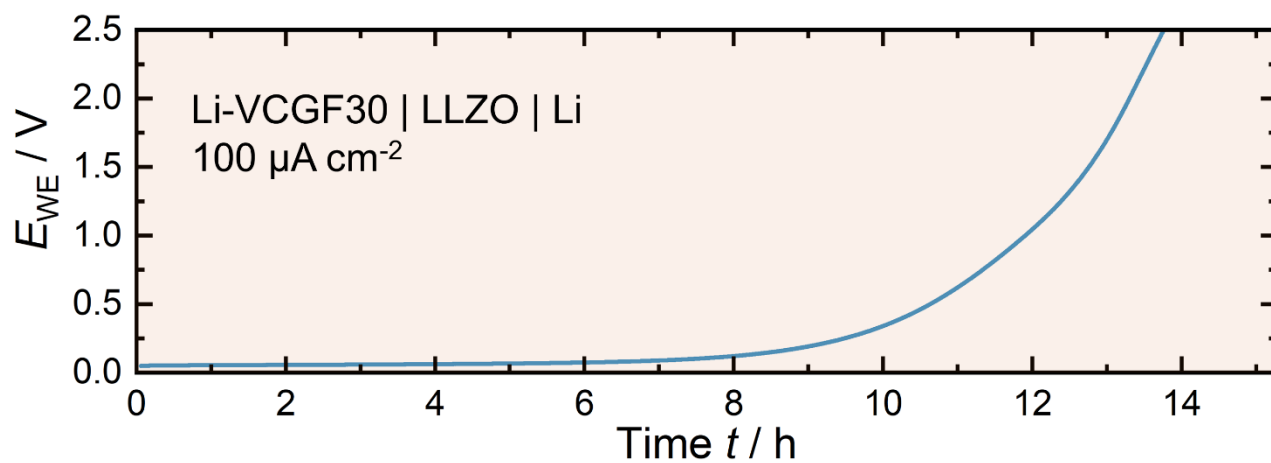
Figure S7. Voltage profile when stripping a Li-VCGF30 composite electrode. The performance is unchanged when compared to pure lithium. This may either be explained by the poor wetting of lithium on VCGF and thus, inhomogeneous distribution thereof, or rather that the VCGF is not capable in the same way of increasing the effective diffusion coefficient and guiding contact like CNTs.

Table S2. Summary of shear (v_s) and longitudinal (v_l) soundwave velocity in the analyzed specimens. Note that due to increasing inhomogeneity of Li-CNT30, shear wave velocity v_s was not assessable from acoustic measurements and was thus estimated to be 2.6 km s^{-1}. Wave speeds were averaged from several measurements on different parts of the analyzed specimens.

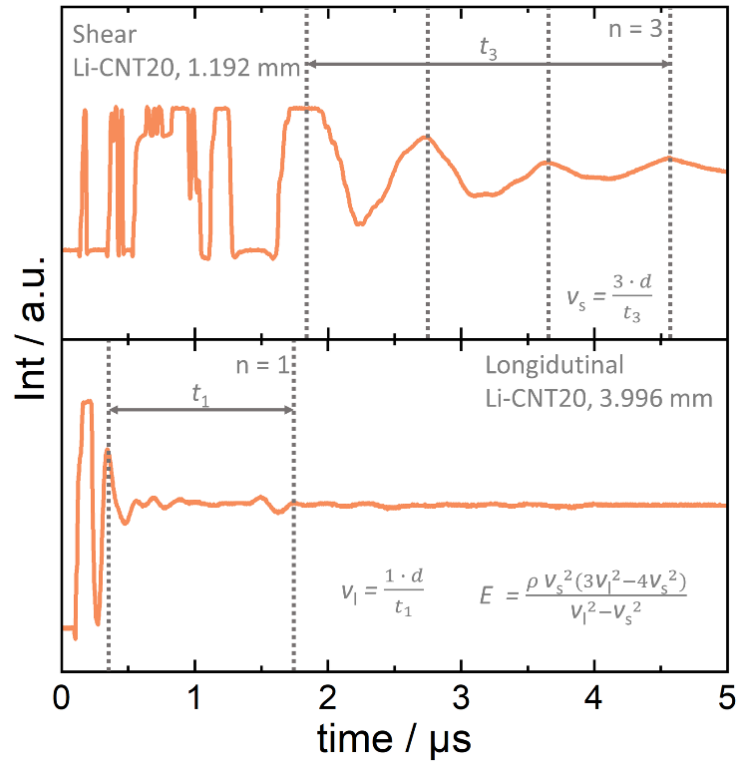| Material	ρ / g cm^{-3}	v_s / km s^{-1}	v_l / km s^{-1}	E / GPa
Li (Ref [6])	0.533	2.30 ± 0.02	5.28 ± 0.26	7.82
Li-CNT10	0.540	2.4 ± 0.1	5.7 ± 0.4	8.97
Li-CNT20	0.581	2.6 ± 0.1	5.7 ± 0.1	10.89
Li-CNT30	0.588	2.6	6.7 ± 0.1	11.23

Figure S8. Example of the data acquisition for speed of sound measurements conducted within this work in the case of Li-CNT20 for shear wave speeds (top) and longitudinal wave speeds (bottom).

Literature

[1]   T. Krauskopf, H. Hartmann, W. G. Zeier, J. Janek, *ACS Appl. Mater. Interfaces* **2019**, *11*, 14463–14477.

[2]   T. Krauskopf, B. Mogwitz, C. Rosenbach, W. G. Zeier, J. Janek, *Adv. Energy Mater.* **2019**, *9*, 1902568.

[3]   L. Stolz, G. Homann, M. Winter, J. Kasnatscheew, *Mater. Today* **2021**, *44*, 9–17.

[4]   H. J. S. Sand, *London, Edinburgh, Dublin Philos. Mag. J. Sci.* **1901**, *1*, 45–79.

[5]   J. T. S. Irvine, D. C. Sinclair, A. R. West, *Adv. Mater.* **1990**, *2*, 132–138.

[6]   A. Masias, N. Felten, R. Garcia-Mendez, J. Wolfenstine, J. Sakamoto, *J. Mater. Sci.* **2018**, *54*, 2585–2600.